JOURNAL OF APPLIED ELECTROCHEMISTRY 18 (1988) 410–416

Performance and impedance studies of thin, porous molybdenum and tungsten electrodes for the alkali metal thermoelectric converter

B. L. WHEELER, R. M. WILLIAMS, B. JEFFRIES-NAKAMURA, J. L. LAMB, M. E. LOVELAND, C. P. BANKSTON, T. COLE

Jet Propulsion Laboratory, California Institute of Technology, 4800 Oak Grove Drive, Pasadena, California 91109, USA

Received 29 April 1987; revised 20 October 1987

Columnar, porous, magnetron-sputtered molybdenum and tungsten films show optimum performance as AMTEC electrodes at thicknesses less than 1.0 μm when used with molybdenum or nickel current collector grids. Power densities of 0.40 W cm^{-2} for 0.5 μm molybdenum films at 1200 K and 0.35 W cm^{-2} for 0.5 μm tungsten films at 1180 K were obtained at electrode maturity after 40–90 h. Sheet resistances of magnetron sputter deposited films on sodium beta″-alumina solid electrolyte (BASE) substrates were found to increase very steeply as thickness is decreased below about 0.3–0.4 μm. The a.c. impedance data for these electrodes have been interpreted in terms of contributions from the bulk BASE and the porous electrode/BASE interface. Voltage profiles of operating electrodes show that the total electrode area, of electrodes with thickness $< 2.0\,\mu$m, is not utilized efficiently unless a fairly fine ($\sim 1 \times 1$ mm) current collector grid is employed.

1. Introduction

The alkali metal themoelectric converter (AMTEC) is a high efficiency, high power density, thermally regenerative, electrochemical system based on sodium ion transport from a high temperature (900–1300 K) liquid sodium reservoir through beta″-alumina solid electrolyte (BASE) to an exterior, sodium permeable electrode from which sodium gas diffuses to a condenser surface at 400–600 K [1–7]. The ratio of the sodium activities in the reservoir and at the electrode give rise to a voltage, and because all transport and electrochemical processes can be made quite efficient, high current densities are possible. Previous work has emphasized porous Mo electrodes of thickness 1.0–3.0 μm which show very high initial power densities but degrade to a 'mature' state with a two to five-fold reduction in power and efficiency after 10–1000 h, the time depending on temperature as well as other factors such as film morphology and degree of oxidation [8, 9]. We have previously shown that the high initial power is the result of sodium molybdate, Na_2MoO_4, formation within the porous electrode, resulting in an enhanced efficiency of sodium transport through the porous electrode. Since Na_2MoO_4 is eventually lost from the electrode by evaporation, current research continues to address AMTEC's only remaining fundamental problem: selection of a long-life ($> 10\,000$ h) electrode with a negligible contribution to the device's internal impedance.

The positive, current-collecting electrode in the AMTEC device must be a good electronic conductor to minimize efficiency losses due to iR drop in this low voltage, high current device. Also, the electrodes should pose little resistance to Na^0 vapor transport away from the BASE. Thus, a very thin electrode would be desirable in connection with an overlying current collection grid. This would minimize resistance due to sodium vapor flow pressure drop, even in an electrode which has lost the sodium ionic conductor Na_2MoO_4 by evaporation. Finally, an overlying current collection grid would be needed to offset the higher sheet resistance in a very thin film. In this paper, we report the results of experiments utilizing very thin ($\leqslant 1\,\mu$m) molybdenum and tungsten electrodes with current collection grids and compare their characteristics with those of thicker electrodes.

2. Experimental details

Very thin Mo and W electrodes were prepared by magnetron sputtering of cylindrical Mo or W targets (99.9%, Sputtered Films, Inc.) onto a masked BASE tube in a method similar to that used to deposit thicker Mo electrodes [8]. Thin (0.13 mm) Mo wire strips, cut to the length of the Mo electrodes, were laid on the tube and were held in place by tying thicker Mo wires (0.5 mm diameter) around the tube in at least four places. The distance between the thin wires was approximately 0.5 mm. A current and voltage probe was tied onto the electrode at the centre with 0.5 mm Mo wire. The length of the electrodes was 0.8–1.6 cm. Since the BASE tube has a diameter of 1.5 cm, the electrode areas were approximately 4.2–8.5 cm^2. An illustration of the electrode and grid is shown in Fig. 1. In some cases, the Mo grids were brazed to

0021-891X/88 $03.00 + .12

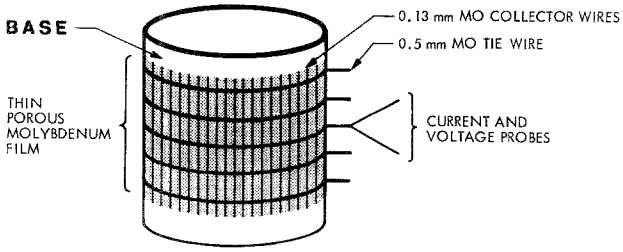

Fig. 1. Scheme of electrode with Mo wire grid.

the electrodes by coating the Mo wires with a braze powder/cement slurry before they were tied on, and then by brazing as described previously [8].

Current collector grids for the W electrode were constructed of a single cylindrical wrapping of expanded nickel mesh (1.27 mm × 0.72 mm diamond grid mesh, original thickness 0.127 mm, Delker Corp.) which was tied in place by loops of 0.5 mm Mo wire separated from each other by about 1.0 mm. Since nickel has a linear thermal expansion coefficient, in K^{-1} (13.3×10^{-6}), substantially greater than those of BASE (7.4×10^{-6}), Mo (5.4×10^{-6}), and W (4.5×10^{-6}), the nickel grid bonded strongly and permanently to both the electrode and tie-wires on heating to AMTEC operation temperatures [10, 11]. Sheet resistance measurements and voltage profiles were obtained on other electrodes which had a current–voltage lead pair to each of two or four brazed 0.5 mm Mo wire contact loops. The current was supplied using a power supply (Kepco model JQE 15-6 MVP, Flushing, NY) and monitored with a digital multimeter. The voltage was measured with a digital multi-function meter. Voltage profiles were obtained on these electrodes by discharging the electrode through one contact while monitoring the voltage at each of the four contacts.

Small patch and ring electrodes with areas of 0.3–1.3 cm^2 were used for a.c. impedance measurements. However, a.c. impedance data of larger electrodes were obtained in some instances.

Current interrupt measurements were carried out by establishing a steady-state current in an electrode and then triggering a fast FET switch with a voltage pulse to interrupt the steady-state current flow. The voltage of the electrode was monitored with a Nicolet digital oscilloscope. The immediate voltage change corresponds to the total ohmic voltage drop within the cell. The remaining voltage difference, with respect to open circuit, is due to concentration polarization and capacitance.

The experiments and equipment used to obtain other data in this paper have been described in detail previously [5, 6, 8, 9].

3. Results and discussion

A compilation of sheet resistance measurements is given in Table 1 for various thicknesses of Mo and W electrodes, both at room temperature and at AMTEC operating temperatures. There are some irregularities, especially among the thinner electrodes, presumably caused by minor variations in the sputtering conditions and the BASE tube surface. The two-probe measurements include the contact resistances between the probes, the braze, and the electrode. Using the data from two-probe and four-probe measurements on the same electrodes, this resistance has been calculated to be in the order of 0.1 ohm per contact. This is somewhat large and in an optimized device, we estimate that it can be reduced by as much as one order of magnitude. Accomplishment of this goal is not complex and the contact resistance can be lowered, by use of more braze, to 0.03 Ω as has been observed previously with thicker electrodes. In the case of the very thin electrodes, however, braze was kept to a minimum in order to perturb less of the electrode area.

At room temperature, the sheet resistance is quite small until the electrodes are 0.5 μm thick. The actual point where the Mo film becomes discontinuous will depend on the surface roughness and cleanliness of the BASE tube and may vary somewhat from tube to tube as well as with sputtering conditions. The high temperature resistivities are significantly larger than those at room temperature. This could be due in part

Table 1. Typical sheet resistances observed for porous, columnar, magnetron sputtered Mo and W films on cylindrical BASE substrates. Four-probe measurements do not include contact resistance, two-probe measurements include contact resistance

Nominal thickness (μm)	*Sheet resistance at 300 K (Ω square^{-1})*	*Sheet resistance at AMTEC operating conditions 1000–1200 K (Ω square^{-1})*
Molybdenum electrodes		
0.15	62.2 four-probe	90 000 four-probe
0.30	2.65 four-probe	4 000 four-probe
0.45	2.67 two-probe	5.9 two-probe
0.5	1.38 four-probe	
0.6	1.12 four-probe	60 four-probe
1.0	0.282 four-probe	
1.4	0.263 four-probe	0.98 four-probe
2.5	0.34 two-probe	0.42 two-probe
Tungsten electrodes		
0.5	2.01 four-probe	6.6 four-probe
1.8	0.60 four-probe	1.88 four-probe

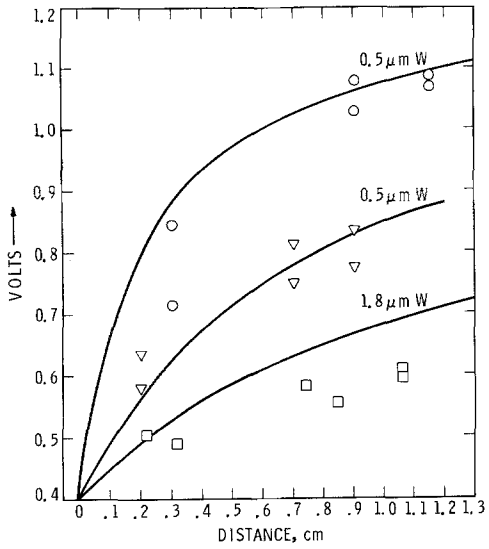

Fig. 2. Experimental and calculated voltage profiles. (○) Measured profile of 0.5 μm W electrode at 1150 K, sheet resistance = 10.9 Ω square^{-1}, G_{fit} = 50. For 0.5 μm W at 1140 K (▽), sheet resistance = 2.4 Ω square^{-1}, G_{fit} = 40. For 1.8 μm W at 1135 K (□), sheet resistance = 1.8 Ω square^{-1}, G_{fit} = 200.

to the positive thermal coefficient of resistivity of the metals and in part due to sintering of the Mo film. The contact resistance is also observed to be at least twice the room temperature value in the AMTEC operating range.

The same electrodes used for four-probe sheet resistance measurements were used for voltage profiling to determine the degree of electrode area utilization. Figure 2 shows experimental voltage profile data for three different tungsten (W) electrodes. Also included are voltage profile curves calculated for these electrodes on the basis of measured film sheet resistance, morphological characteristics estimated from scanning electron microscopy, BASE resistance, and equations for the sodium pressure at the exterior surface of the electrode and pressure gradient within the electrode based on the kinetic theory of gases [2, 5, 12]. The equation used to calculate the local voltage–current density relation includes contributions from the ohmic drop due to the ionic resistance of BASE, R_{BASE}; the sodium vapor pressure due to the condenser, P_1; the pressure due to current flow, P_i; the pressure gradient within the electrode pores, ΔP; and the liquid sodium reservoir pressure, P_2.

$$V = -(RT_2/F) \ln\left(\frac{P_1 + P_i + \Delta P}{P_2}\right) + jR_{BASE} \quad (1)$$

R is the gas constant, F is the Faraday number, T_2 is the temperature of the electrode segment of the BASE tube, and j is the current density. Expressions for P_i and ΔP have previously been reported [2, 5].

$$P_i = (2\pi MRT)^{1/2} j/F \quad (2)$$

$$\Delta P = 3/4 \left(\frac{RT}{2\pi M}\right)^{1/2} G \frac{Mj}{F} \quad (3)$$

M is the atomic weight of sodium and G, in the second expression, is a dimensionless constant expressing the morphology of the electrode.

$$G = \frac{l}{a^3 N} \quad (4)$$

where l = pore length, a = pore radius and N = number density of pores.

The current–voltage curves characteristic of typical thin Mo electrodes with current collecting grids are not significantly different from those of thicker Mo sputter-deposited films. The appearance of the current–voltage characteristic is quite insensitive to morphology or thickness of the electrode. The current and power densities of a very thin electrode without a collector grid will be smaller than those of one with a grid. With the higher sheet resistance of very thin electrodes, the area surrounding the current collector that is effectively utilized will be smaller. Therefore, a very thin electrode must have a collector grid with a characteristic grid spacing which will optimize the effective area of the electrode utilized and the effective sheet resistance of the grid/film combination.

Higher power densities, obtained with very thin Mo electrodes having collector grids, can be expected from the reduced Na^0 vapor diffusion resistance and the collector grid offsetting the increase in electrode sheet resistance. Very thin electrodes will exhibit degradation with time that is much less dramatic than that of thicker Mo electrodes. Unlike the thicker electrodes which typically show decay in power density to 20–30% of the initial value [8], a 0.5 μm Mo electrode had a power density of 80% of initial after almost 100 h (Fig. 3), and was significantly higher in power than an otherwise similar 1.0 μm Mo electrode. In Fig. 4, the power densities of 1.8 and 0.5 μm W electrodes are shown with respect to time. In this case also, it is clear that thinner sputtered W electrodes with current collector grids and otherwise similar columnar morphology show superior performance. In this paper, the initial degradation processes will not be addressed in detail, but an important point can be stated here. The effects of Na_2MoO_4 or Na_2WO_4 in very thin electrodes will be minimized, since (a) less will be present to begin with and it will be lost quickly, and (b) its enhancing effect over pure sodium vapor flow will be less since the vapor flow pressure drop has

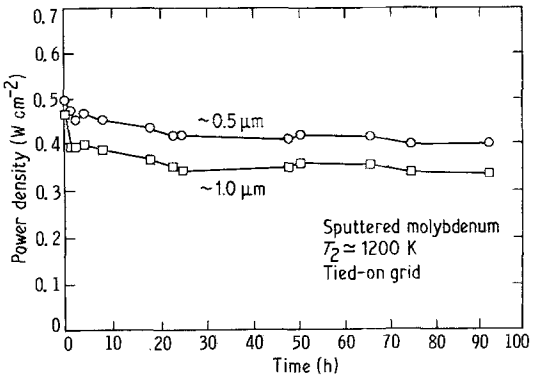

Fig. 3. Power densities vs time for 1.0 and 0.5 μm Mo electrodes. (○) 0.5 μm electrode data, (□) 1.0 μm electrode data.

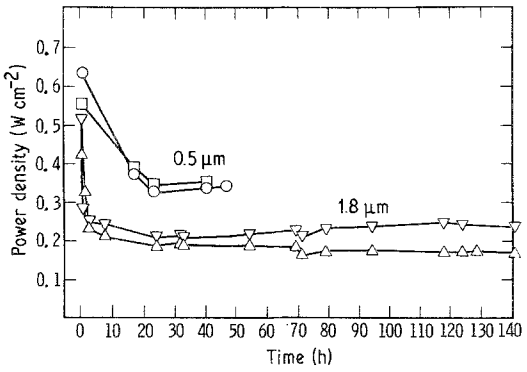

Fig. 4. Power densities vs time for 1.8 and 0.5 μm W electrodes. (○, □) 0.5 μm electrode data, (△, ▽) 1.8 μm electrode data.

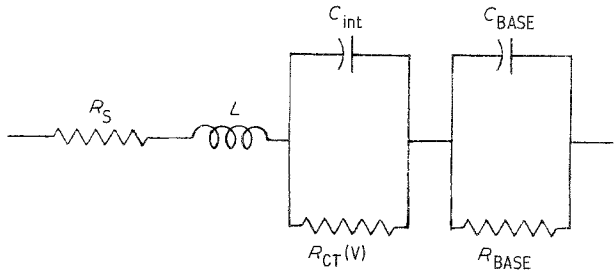

Fig. 6. Equivalent circuit for the AMTEC cell. R_S and L are series resistance and inductance. R_{BASE} and C_{BASE} are the bulk ionic resistance and bulk capacitance of the solid electrolyte. R_{CT} (V) is the potential dependent charge transfer resistance of the solid electrolyte and C_{int} is the interfacial capacitance.

been substantially reduced. A detailed description of the effects of Na_2MoO_4 and Na_2WO_4 on the performance of Mo and W electrodes is discussed elsewhere [8, 9, 13].

A.c. impedance experiments on these thin electrodes have allowed many features of the equivalent circuit to be determined. The a.c. impedance of a 0.6 μm molybdenum electrode at d.c. cell biases from open-circuit (+1.25 V vs Na) to near short circuit (+0.1 V vs Na) is shown in Fig. 5. Because of the experimental arrangement in which the Na reservoir is grounded, the Mo electrodes were the counter and reference electrodes and the Na was the working electrode in a two-electrode configuration. An equivalent circuit for the device can be determined from the impedance spectra. This circuit is shown in Fig. 6.

R_S is a combination of all resistances in the device which are in series with the other circuit elements. This includes lead resistance, contact resistance of the leads to the Mo film electrode and part of the sheet resistance of the electrodes. This value was potential independent as expected for purely ohmic resistances and had a value of 1.0 ± 0.1. It is obtained from the high frequency real axis intercept divided by the area of the electrode (by which the values have been normalized). The cell bias can be converted to a potential vs Na/BASE by adding the product of the cell current and R_S plus R_{BASE} to each cell voltage value. The sheet resistance of the electrode can be thought of as a parallel combination of ever increasing resistances as the distance from the contact increases. However, since it is a parallel combination, the equivalent resistance seen with the a.c. impedance experiment will in the first order, be independent of the electrode sheet resistance. The higher the sheet resistance, the lesser of the electrode area will be effectively used.

An inductance is also found to be present and is caused by the ringlike nature of the contact and electrode film around the tube filled with metallic

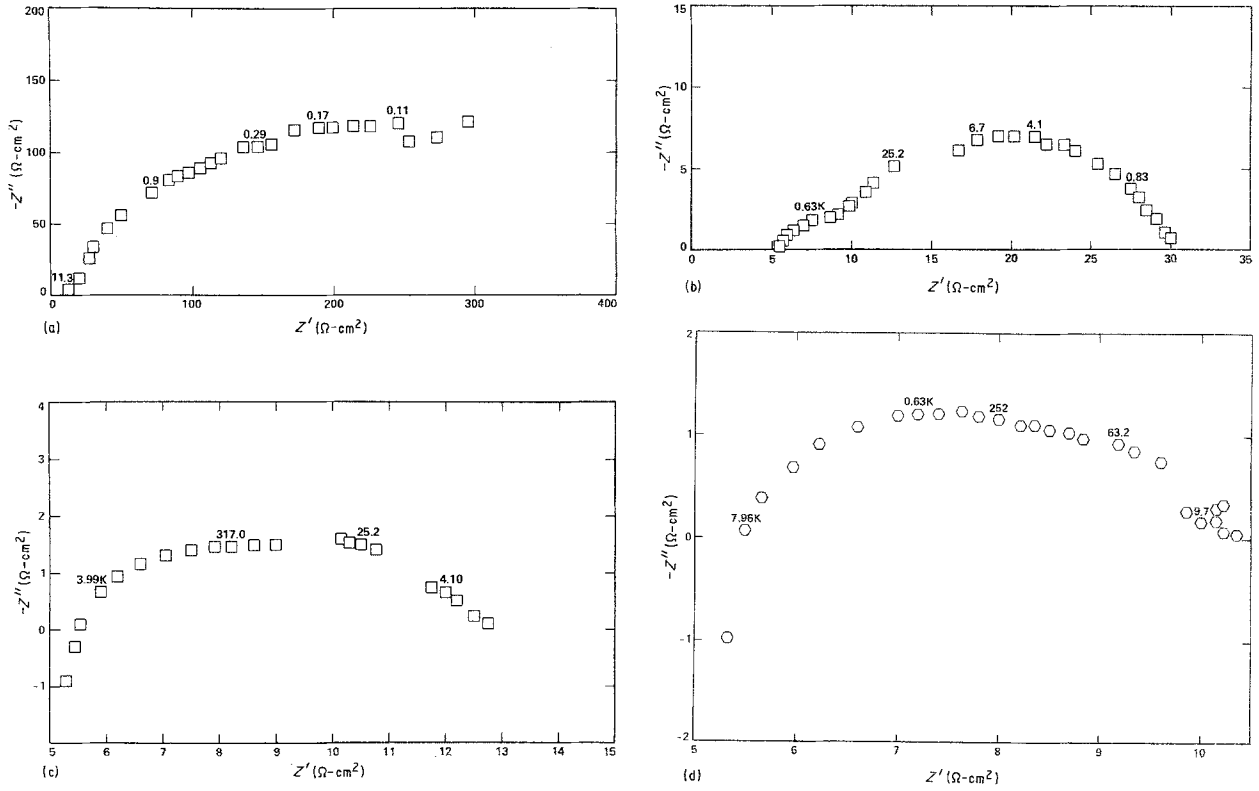

Fig. 5. A.c. impedance data for a 0.6 μm Mo electrode on BASE at 970 K. (a) 1.20 V, (b) 0.80 V, (c) 0.40 V, (d) 0.10 V.

Table 2. Parameters used to fit a.c. impedance data for 0.6 μm Mo electrode on BASE at 970 K

E (*est.*) *vs* *Na/BASE*	*Cell voltages*	*1st loop BASE/ionic conductor*		*2nd loop interface*	
		R ($\Omega\ cm^{-2}$)	C ($\mu F cm^{-2}$)	R ($\Omega\ cm^{-2}$)	C ($F cm^{-2}$)
1.20	1.20	3.3	250	70	1.5×10^{-2}
0.92	0.80	3.3	310	19	8.2×10^{-3}
0.73	0.40	3.1	300	3.5	2.1×10^{-2}
0.67	0.10	3.5	370	2.4	4.8×10^{-3}

sodium. Assuming a series inductance, L, the positive imaginary values can be fit to $Z'' = 2\pi fL$ where Z'' is the imaginary value of the impedance and f is the a.c. frequency. This value is calculated to be 8 μH and is potential independent, as expected. It is too large to be caused by just the one coil of contact wire and is therefore probably a parallel combination of inductances from the electrode itself. The a.c. impedance spectra generally contain two loops which correspond to two R–C combinations in series. The values of R can be determined from the diameter of the semicircle along the real axis. The value of C can be conveniently determined from $2\pi f_0 = (RC)^{-1}$, where f_0 is the frequency of the values which lie at the top of the semicircle, and R is the resistance determined as just described. The values of R and C for the two loops are shown in Table 2 for a variety of thin Mo electrodes. It can be seen that the R for the first loop and both C values are relatively independent of voltage, whereas the R for the second loop decreases toward short-circuit. As the time constant of the second loop approaches that of the first, the values of R and C become more difficult to extract, and therefore more uncertain. The potential independent first loop is almost certainly due to the BASE with contributions from ionic conductors which may be present in the electrode. However, it strongly depends on the history of the BASE tube and was often not resolvable at high temperature for electrodes on fresh tubes with minimum prior exposure to air due to the small ideal value of R, $\sim 0.2\,\Omega\text{-cm}^2$. Also, when the area of the electrode is not utilized efficiently, the normalization of resistance with respect to electrode area magnifies the computed ionic resistance. The high frequency, potential independent semicircle was more often observed at lower temperatures where the BASE resistance is higher. The equivalent circuit for BASE has been shown previously [14] to include a non-Debye capacitance or a constant phase angle element which does not obey the usual relationship between the impedance of a capacitor and f^{-1}, but a relationship to f^{n-1} where $0 < n < 1$. This has the effect of moving the center of the semicircle to negative values of $-Z''$. Both of the RC loops in the data shown here have centres which lie below the real axis. The second loop has an R which decreases as the faradaic current increases toward short-circuit and it is therefore assigned as a charge transfer resistance. The slower heterogeneous charge transfer is almost certainly the reduction of Na^+ at the Mo electrode. Therefore, the features which are visible by a.c. impedance are lead and contact resistances, electrode inductance, Na^+ ion transport through the BASE, and heterogeneous charge transfer at the Mo electrode.

An exactly analogous assignment of the a.c. impedance data of thin W electrodes can be carried

Table 3. Parameters used to fit a.c. impedance data of W electrodes

Electrode thickness (*μm*)	T (*K*)	E (*est.*) *vs* *Na/BASE*	j ($A\ cm^{-2}$)	R (Ω-cm^2)	C ($\mu F cm^{-2}$)
0.5	818	0.920	3.37×10^{-4}	350	1388
		0.752	3.56×10^{-3}	37.6	1364
		0.609	1.92×10^{-2}	5.33	1492
		0.456	1.12×10^{-1}	0.841	1262
	990	0.944	6.10×10^{-2}	2.86	1755
		0.716	2.89×10^{-1}	0.504	678
		0.449	1.15	0.165	1288
		0.353	1.93	0.075	3128
	1103	1.301	1.86×10^{-3}	36	88.4
		1.020	4.69×10^{-2}	2.38	211
		0.941	9.54×10^{-2}	1.13	281
		0.710	4.89×10^{-1}	0.341	282
1.8	1093	1.301	7.96×10^{-4}	42.7	455
		1.043	3.45×10^{-2}	3.64	346
		0.908	1.22×10^{-1}	1.205	322
		0.729	4.06×10^{-1}	0.226	559

Table 4. Internal ohmic resistances of molybdenum and tungsten electrodes, measured by current interrupt; t *is time at high temperature*

Thickness	T (*K*)	t (*h*)	R ($\Omega\ cm^{-2}$)
W, 1.8 μm	1188	4	0.737
W, 1.8 μm	1188	76	0.835
W, 0.5 μm	1183	24	0.571
Mo, 2.5 μm	1123	177	0.237
Mo, 0.45 μm	1120	177	0.565

out. Table 3 shows the parameters used to fit the data for W electrodes of various thicknesses, temperatures, and potentials. Higher frequency *RC* loops due to bulk BASE could not be adequately resolved from the low frequency loops in these cases. The high capacitances of the lower temperature data for the 0.5 μm electrode, obtained during initial warm-up, are presumably due to the presence of small amounts of oxide phases, in particular Na_2WO_4, in the porous tungsten electrode. This ionic conducting compound may increase the capacitance by increasing the effective ionic conductor/metal interface area. In principle, these data may be used to obtain kinetic information about the sodium ion–electron recombination reaction at the metal–BASE interface.

Because the a.c. impedance measurements are carried out in a two-electrode configuration, and power curves in a four-probe configuration which does not eliminate internal ohmic resistance, corrections must be made for *iR* drop to both sets of measured electrode potentials in order to obtain true potentials vs the Na/BASE reference potential reported here. Table 4 shows internal ohmic resistances obtained from current interrupt experiments in a four-probe configuration. Furthermore, concentrations or activities of Na^+ and Na^0 at the interface are either unknown or at best crudely estimable. For example, the morphological parameters of the electrode, the sodium flux, and the condenser temperature can be used to estimate the sodium pressure at the interface as the sum of three terms: the pressure of sodium at the condenser, the pressure of sodium at the electrode surface due to the flux, and the pressure gradient in the pores due to the flux and morphological factors. Finally, since the active portion of the porous electrode/BASE interface is actually the three-phase boundary between metal, BASE, and vacuum, the appropriate area to use in deriving kinetic parameters is related to the total length of this boundary, which cannot easily be measured. Figures 7 and 8 show fracture cross-sections and surface views of Mo and W electrode

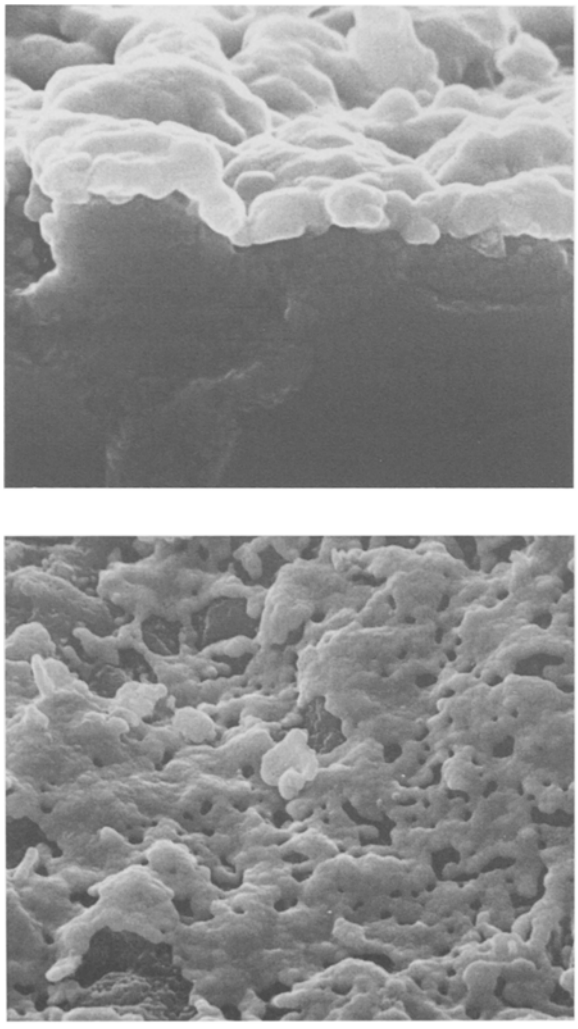

Fig. 7. (Top) Fracture cross-section of 0.5 μm Mo electrode film, 16.9 kX. (Bottom) Surface view of 0.5 μm Mo electrode film, 4.2 kX.

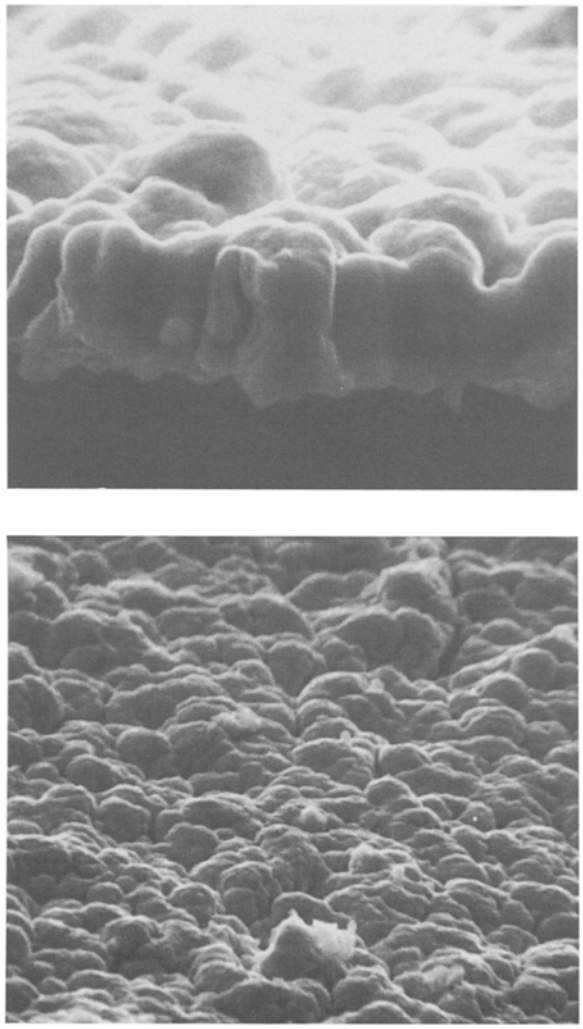

Fig. 8. (Top) Fracture cross-section of 1.8 μm W electrode film, 9.7 kX. (Bottom) Surface view of 1.8 μm W electrode film, 4.2 kX.

films following high temperature operation in the AMTEC cell. The morphology is very complex, and the interfacial region is often damaged when fractured. Typically, electrodes are 10–20% porous and the films exhibit a columnar morphology with clumps of columns grouped together with larger cracks or pores between the clumps.

4. Conclusions

Thin, porous Mo films show promise as electrodes in the AMTEC device. The thin films have reduced Na^0 vapor flow impedance. The increased sheet resistance of the electrodes can be offset by the use of current collector grids. The current–voltage behavior appears similar to that of thicker Mo electrodes, but larger power densities and short-circuit current densities are obtained for mature electrodes. A.c. impedances can be used to obtain the resistances due to the contacts and leads, the inductance of the electrode, information about the Na^+ ionic transport in the BASE, as well as kinetic/concentration information about the reduction reaction of Na^+ at the Mo electrode. However, a.c. impedance is not useful in determining sheet resistances in the thin Mo films.

Sheet resistances measurements show a large increase for thicknesses less than $\sim 0.5\,\mu$m. The lowest practical thickness porous electrode has not been determined, but it is evident that films much less than $0.5\,\mu$m thick would require very fine current collector grids, perhaps prepared by photolithographic techniques.

Acknowledgements

The research described in this paper was performed by the Jet Propulsion Laboratory, California Institute of Technology, and was supported by the US Army Tank Automotive Command, the National Aeronautics and Space Administration, the Department of Energy's Sandia National Laboratories, Albuquerque, and the Office of Innovative Science and Technology/ Strategic Defense Initiative Organization. The authors wish to acknowledge useful discussions with Drs J. Kummer, N. Weber and J. Lambe.

References

[1] N. Weber, *Energy Convers.* **14** (1974) 1.
[2] T. Cole, *Science* **221** (1983) 915.
[3] T. K. Hunt, N. Weber and T. Cole, in 'Solid State Ionics', Vol. 5, (edited by J. B. Bates and G. Farrington), North Holland Publishing Co., Amsterdam (1981) p. 263.
[4] T. K. Hunt, N. Weber and T. Cole, in 'Proceedings of the 13 Intersociety Energy Conversion Engineering Conference', SAE, Warrendale, PA (1978) p. 2011.
[5] C. P. Bankston, T. Cole, R. Jones and R. Ewell, *J. Energy* **7** (1983) 442.
[6] C. P. Bankston, T. Cole, S. K. Khanna and A. P. Thakoor, in 'Space Nuclear Power Systems 1984', Vol. II (edited by M. S. El-Genk and M. D. Hoover), Orbit Book Co., Malabar, FL (1985) p. 393.
[7] C. P. Bankston, in 'Space Nuclear Power System 1986' (edited by M. S. El-Genk and M. D. Hoover), Orbit Book Co., Malabar, Fl, (1987) p. 199.
[8] R. M. Williams, G. Nagasubramanian, S. K. Khanna, C. P. Bankston, A. P. Thakoor and T. Cole, *J. Electrochem. Soc.* **133** (1986) 1587.
[9] R. M. Williams, C. P. Bankston, S. K. Khanna and T. Cole, *J. Electrochem. Soc.* **133** (1986) 2253.
[10] G. J. Tennenhouse, R. C. Ku, R. H. Richman and T. J. Whalen, *Am. Ceram. Soc. Bull.* **54** (1975) 523.
[11] R. E. Bolz and G. L. Tuve (eds), 'CRC Handbook of Tables for Applied Engineering Science', CRC Press, Boca Raton, FL (1973) p. 117.
[12] E. H. Kennard, 'Kinetic Theory of Gases', McGraw-Hill, New York (1938) p. 304.
[13] R. M. Williams, B. L. Wheeler, B. Jeffries-Nakamura, M. E. Loveland, C. P. Bankston and T. Cole, 'Effects of Na_2MoO_4 and Na_2WO_4 on Thin, Porous Mo and W Electrodes for the Alkali Metal Thermoelectric Converter', submitted for publication.
[14] H. Engstrom, J. B. Bates, W. E. Brundage and J. C. Wang, *Solid State Ionics* **2** (1981) 265.